The Hybrid X-Pinch as a Source of XUV Radiation

Vera M. Romanova, Ivan N. Tilikin, Tatiana A. Shelkovenko, Albert R. Mingaleev, Evgeniy A. Bolkhovitinov, Alexandr A. Rupasov, Alexey E. Ter-Oganesyan, and Sergey A. Pikuz

***Abstract*— The first detailed study of hybrid X-pinch (HXP) radiation in the wavelength range 10–200 Å on the BIN pulser (270 kA, 100 ns rise time) is presented. X-pinch loads were made from Al, Mo, Ag, and W wires with 13–30 μm diameters. Time-integrated images were obtained using open pinholes with 100 μm aperture. Spatially resolved XUV spectra were recorded using a transmission grating spectrograph on UF-4 film and with Fuji TR image plates. Signals from calibrated photoconducting detectors enabled estimates of the absolute yield of radiation and showed that Mo HXPs radiate about 100× more energy in UV radiation than in X-rays with energy above 1 keV.**

***Index Terms*— Hot spot (HS), imaging plates (IPs), soft X-ray (SXR), transmission grating spectrograph (TGS), X-pinch, XUV.**

I. Introduction

X-PINCHES are well-known sources of soft and hard X-ray radiation [1]–[5], with both standard and hybrid configurations being regularly used to explore the radiative properties of high-energy density plasmas [2] as well as for point projection radiography [3]. Qualitative studies of the UV/XUV emission from standard X-pinches was carried out by pinhole imaging, transmission grating spectrometry, and filtered photoconducting detectors (PCD) measurements. They showed strong XUV emission from a region less than 1 mm around the wire crossing point. This makes an X-pinch applicable in new diagnostics, such as a source for XUV absorption spectroscopy or, using radiation lines, a source for scattering experiments. To date, however, XUV measurements do not exist for hybrid X-pinches (HXPs), which are generally much easier to load than standard X-pinches and enable a larger variety of source materials to be used. It is also not clear what pulser parameters are optimal for driving HXPs for generation of XUV radiation, in contrast to producing soft X-ray (SXR) radiation in X-pinch hot spots (HSs), where the guideline $dI/dt > 1$ kA/ns was discovered by Shelkovenko *et al.* [4] a decade ago.

Manuscript received December 25, 2017; revised April 4, 2018, May 22, 2018, and July 5, 2018; accepted August 27, 2018. This work was supported in part by an agreement with Cornell University under NNSA/DOE Cooperative Agreement DE-NA0003764 and in part by the Russian Fund for Basic Research under Grant 17-02-00391. The review of this paper was arranged by Senior Editor F. Beg. *(Corresponding author: Vera M. Romanova.)*

The authors are with P. N. Lebedev Physical Institute of Russian Academy of Sciences, Moscow 119991, Russia (e-mail: vmr@inbox.ru; ivan.tilikin@gmail.com; tchel55@mail.ru; albert99@inbox.ru; bolevar@sci.lebedev.ru; rupasov @sci.lebedev.ru; ter1979@gmail.com; pikuz@mail.ru).

Color versions of one or more of the figures in this paper are available online at http://ieeexplore.ieee.org.

Digital Object Identifier 10.1109/TPS.2018.2870321

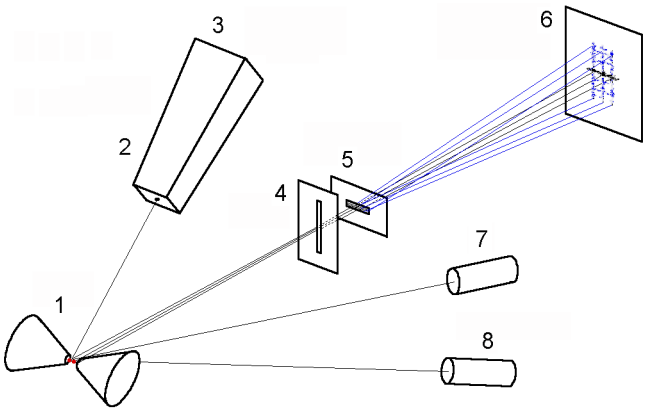

Fig. 1. Experimental setup. 1—HXP. 2—OP. 3—Kodak DR50 film or Fuji TR image plate. 4—Imaging slit. 5—Transmission grating. 6—UF-4 film or Fuji TR image plate. 7 and 8—Diamond PCDs filtered for SXRs or XUV.

II. Experimental Setup

The experiments were performed on the BIN facility with a load current up to 270 kA and a current rise time of about 100 ns. The experimental setup is shown in Fig. 1.

The radiation from HXPs with wires of 13–30 μm diameters of different materials (Al, Mo, Ag, and W) was studied. X-pinch images were obtained using open pinholes (OPs) (pinhole camera without filter) with 100 μm aperture. In first experiments, images were recorded on Kodak DR50 film. This film is characterized by a low sensitivity to the hard radiation ($E > 10$ keV) and visible light. In addition, the pinhole itself served as a diffractive filter with a cutoff energy of approximately ≈60 eV. This film has a protective coating, so the radiation was recorded in the SXR range (1–10 keV) and in the "carbon window" (200–280 eV). In the following experiments, films was replaced by Fuji BAS TR image plates (IPs), which do not have a protective layer and are sensitive over a wider energy band. The temporal parameters of the radiation were studied using diamond PCDs both with and without filters. PCDs have a constant sensitivity over the energy range 10 eV $< E <$ 4 keV, smoothly falling to about zero in the range 15–20 keV.

X-pinch spectra were studied using a transmission grating spectrograph (TGS) [6]. A TGS generally covers a sufficiently wide spectral range (from 10 to 300–600 Å depending on grating parameters) and has a linear dispersion throughout the operating range. The efficiency of transmission gratings (the fraction of energy going into the certain diffraction order) is constant if the bars of the grating are opaque to the

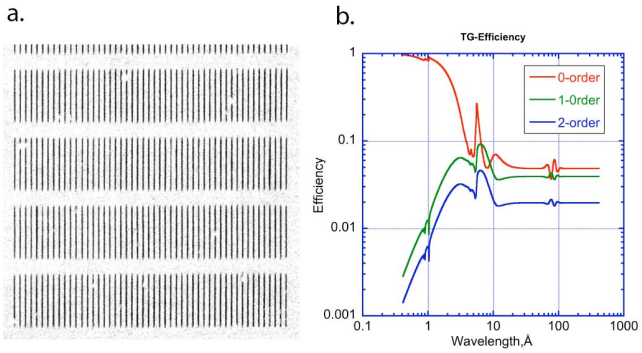

Fig. 2. (a) Image of a portion of the transmission grating and (b) spectral efficiency in the zero, first, and second orders of diffraction.

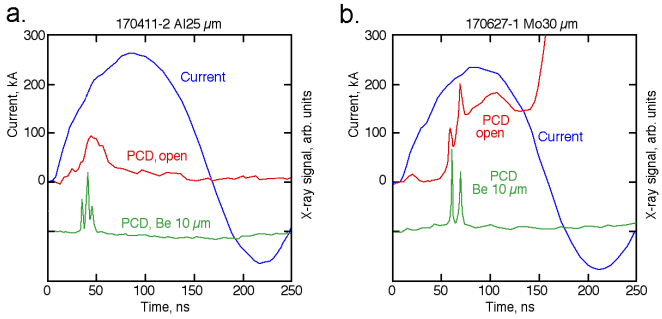

Fig. 3. Examples of current, SXP, and XUV scope signals for Al (25 μm wire) and Mo (30 μm wire) HXPs.

radiation [7]. An important advantage of the transmission gratings, which favorably distinguishes them from the reflective gratings, is the absence of a complicated alignment procedure, as well as the fact that a spectrograph based on such gratings is small and is easily mounted onto a vacuum chamber.

The grating used in the experiments was made from gold and had 50 equidistant slits (slit width $\delta = 0.35$ μm; grating period $d = 1.4$ μm) made in a 0.07×1.7 mm^2 rectangular aperture [Fig. 2(a)]. Slits were oriented along the long side of the aperture. The spectral efficiency of the grating in different diffraction orders depends on aspect ratio $t = \delta/d$ and the grating bar transmission (the grating substrate in our case). For $t = 0.25$ and gold substrate thickness 0.5 μm, the grating efficiency calculated using X-ray database [8] is shown in Fig. 2(b). In the spectral range of our interest ($\lambda > 10$ Å), this grating is effective in the first two orders of diffraction m. For higher orders, the efficiency is small, but it must be taken into account in the complete spectrum analysis. The spectrograms recorded in the experiments are the result of a superposition of the grating-order contributions with relative intensity $I_2/I_1 = 0.5$; $I_3/I_1 = 0.11$; and $I_5/I_1 = 0.04$. The intensities of the 4th, 8th, and 12th... orders for the grating with $t = 0.25$ are zero. As the first stage of data analysis, the full-recorded spectra including all orders were used to estimate the total energy yield of the HXPs in the range 10–400 Å. Later, to unfold the actual spectral distribution, the iterative approach developed in [9] will be used.

It should be noted that in the wavelength range $\lambda < 10$ Å, the grating efficiency varies greatly with wavelength due to the partial transparency of the grating bars [Fig. 2(b)]. Since in the X-pinch radiation the fraction of SXRs is significant, its contribution to the higher orders of the resulting spectrum must be taken into account.

The diffraction limit for a grating resolving power $\lambda/\Delta\lambda_D = N$ (where N is the number of grating lines) is independent of the wavelength. Then the spectral resolution $\Delta\lambda_D$ for $\lambda = 100$ Å and $N = 50$ is 2 Å. However, in a real spectrograph, there is no radiation focusing, so the geometric factors are also essential. The geometric spectral resolution $\Delta\lambda_g$ is determined by $\Delta\lambda_g = d \times [D/b + (r+D)/a]$ from [10]. Here, D is the total aperture of the grating, a and b are distances from the grating to the radiation source and from the grating to the spectrum detection plane, respectively, and r is size of the radiation source. The spectrograph had $D = 70$ μm, r was estimated to be 100 μm, and the experiment distances were $a = 60$ cm and $b = 50$ cm, from which we obtain $\Delta\lambda_g \approx 6$ Å.

The transmission grating has no astigmatism, and this allows one to realize the spatial resolution of the object in the direction perpendicular to dispersion, and simultaneously in the entire working spectral range. For this purpose, an additional slit (4) with width $h = 100$ μm was placed in front of the grating (5) perpendicular to the bars (Fig. 1). As a result, spectra with spatial resolution over the entire length of the HXP were obtained. Under the experimental conditions, the spatial resolution of the object $\Delta l = h \times (a + b)/b$ was 220 μm.

The spectra were recorded either on UF-4 photograph film specially designed for the XUV spectral range [11], or on the Fuji BAS-TR IPs. Unfortunately, reliable data for the IP calibration in XUV energy band do not exist. Our investigation (a description of which is beyond the scope of this paper) showed that IPs used in our experiments are sensitive at least up to a wavelength of 200 Å [12]. The use of the IPs instead of photograph films has advantages described later, and a significant part of the experiments was performed using IPs. However, the films were calibrated, and could be used for absolute measurements and, probably, for IP calibration.

III. Experimental Results

Fig. 3 presents the examples of current and PCD signals in experiments with Al and Mo HXPs. In these experiments, the development of HSs [2], [4] was observed and short pulses (~1–2 ns) of SXR were generated. The radiation recorded by the open PCDs had a duration comparable to the duration of the current pulse. At the late stage of the Mo HXP ($t > 150$ ns), a fast increase of PCD signal was observed [Fig. 3(b)]. The nature of this increase is not yet fully understood but most likely, it is due to the breakdown of the surface of PCD under the action of a pinch radiation. Later this problem was solved.

The total energy yield according to open PCD data was estimated to be 3 J for Al and 6 J for Mo HXPs. In the SXR spectral band ($E > 1$ keV), the energy yield did not exceed about 25 mJ for Al and 100 mJ for Mo HXPs.

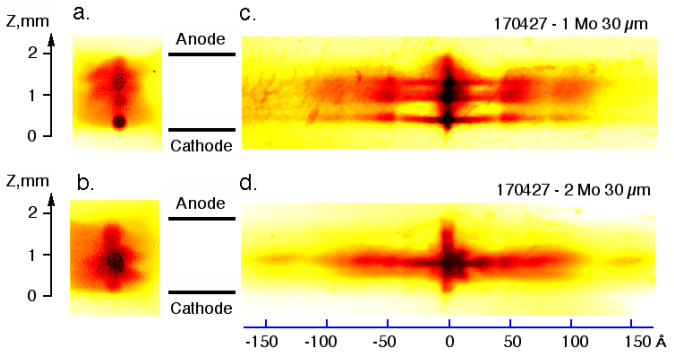

Fig. 4. (a) and (b) OP images recorded on Kodak DR50 film. (c) and (d) Corresponding TGS spectra recorded on UF-4 film from two tests with 30 μm Mo HXPs. Electrodes positions are shown by black solid lines.

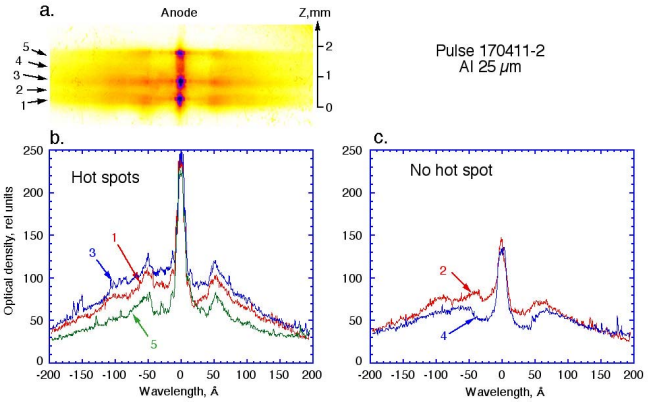

Fig. 5. (a) TGS spectra from a 25-μm Al HXP recorded on UF-4 film and spectrum lineouts [the location number of which corresponds to the position numbers in (a)]. (b) HXP zones with HSs (1, 3, 5). (c) Zones without HSs (2, 4).

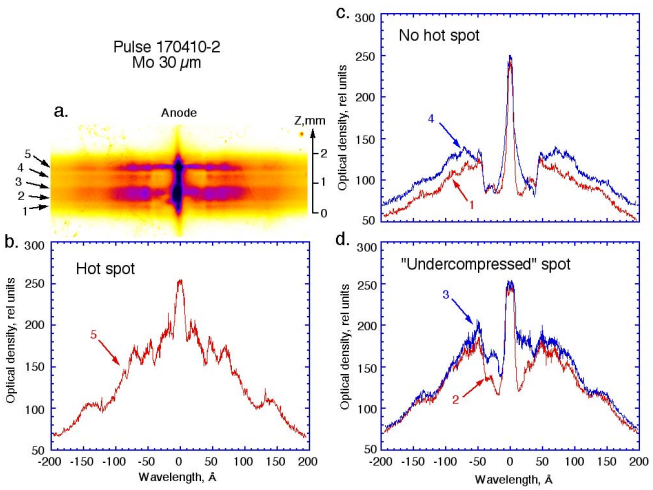

Fig. 6. TGS spectrum from a 30-μm Mo HXP recorded on (a) UF-4 film and spectrum lineouts [the location number of which corresponds to the position numbers in (a)]. (b) HXP zone with a HS (5). (c) Zones without HSs (1, 4). (d) Zones with "undercompressed" HSs (2, 3).

Fig. 4 shows OP images and TGS spectra of Mo HXPs recorded on the film. The radiating area of the HXP usually completely fills the space between electrodes and has complicated structure. There are three visually different zones of the pinhole images: type 1—small very bright spots (BSs) with size less than diameter of the pinhole aperture ($\ll$100 μm); type 2—BSs with size comparable with the pinhole aperture; and type 3—diffuse larger size regions ($\gg$100 μm) that radiate weakly across the entire gap. XUV spectra obtained by the TGS with slit generally show the same structures as OP images. It can be clearly seen that the three bright areas in Fig. 4(a) correspond to three bright TGS spectra [Fig. 4(c)] and one bright area in Fig. 4(b), corresponds to one bright spectrum in Fig. 4(d). However, in the second case, the OP image of the small radiating area of type 1 is surrounded by a diffuse image of type 2. The nature of these bright areas will be discussed further.

There are two terms often used to specify bright radiating areas: BS and HS, which are understood as synonyms. But as was described in detail in review [2], the BS and HS in an X-pinch are the objects of essentially different physical nature. HSs appear as a result of the deepest compression of the X-pinch load and are characterized by extremely high parameters: micrometer or even submicrometer size, an electron temperature in the kilo electronvolts range, and an ion density which may exceed the solid matter density. A characteristic feature of the HS is intense continuum in a short wavelength part of the SXR spectral band (photon energy $E > 2.5$–3 keV). Only HSs are able to work as ideal (with micrometer spatial and picosecond temporal resolution) radiation sources for point-projection radiography [3]. The BS is the plasma that may not have undergone a "final" extreme compression, namely, it does not reach micrometer-scale dimensions. The BSs can have high temperature, a high total emission yield and radiate over a wide spectral band. In that sense BS, is a more general term describing a wide range of pinched plasma parameters. The total amount of energy emitted from the BS can be larger than that of the HS, but mostly in line radiation, not in the SXR band continuum. It makes sense to distinguish the intermediate class of "undercompressed" HS. Plasma parameters in this category of HSs, mainly plasma density, do not reach the level necessary for the formation of a HS in terms of the brightness and size, but such an object can be an effective, compact source of intense radiation in the XUV range of interest here.

Figs. 5–8 present a series of HXP radiation spectrograms with spatial resolution produced by the TGS on photograph film, as well as the density profiles ("lineouts") along dispersion direction. Each lineout corresponds to a specific crossection of the X-pinch spectrum and the lineouts are grouped according to definition of X-pinch zones presented in the previous paragraph: 1) with HSs; 2) without HSs; and 3) with "undercompressed" HSs. The characteristic intensity dip within the range from 17 to 44 Å is related to the carbon absorption K-edge of the film emulsion and protective layer [12]. Particular transitions in the spectra (individual spectral lines) could not be resolved because of the low resolving power of the TGS used in the experiments. The averaged peaks in the spectrograms correspond to the different

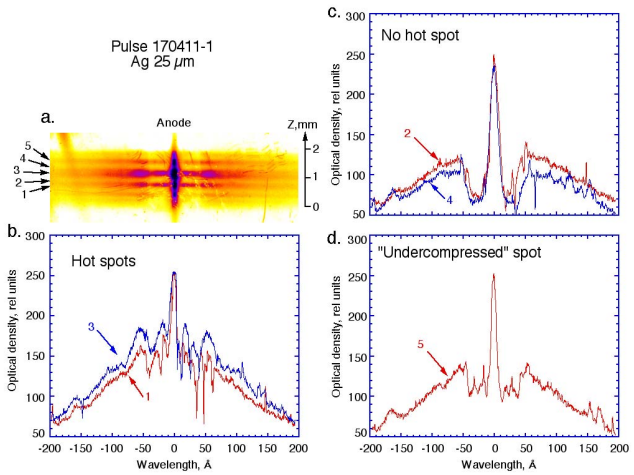

Fig. 7. TGS spectrum from a 25-μm Ag HXP recorded on (a) UF-4 film and spectrum lineouts [the location number of which corresponds to the position numbers in (a)]. (b) HXP zones with HSs (1, 3). (c) Zones without HSs (2, 4). (d) Zone with "undercompressed" HS (5).

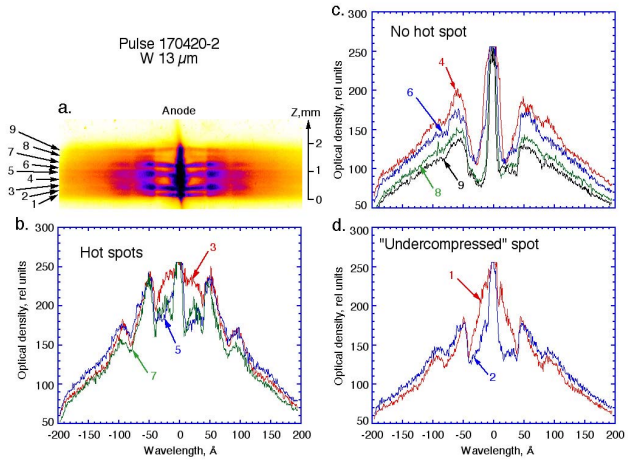

Fig. 8. TGS spectrum from a 13-μm W HXP recorded on (a) UF-4 film and spectrum lineouts [the location number of which corresponds to the position numbers in (a)]. (b) HXP zone with HSs (3, 5, 7). (c) Zones without HSs (4, 6, 8, 9). (d) Zones with "undercompressed" HSs (1, 2).

groups of *K*-, *L*-, and *M*-transitions of the X-pinch plasma ions of the elements used as the loads.

Spectrograms contain short-wave regions (adjacent to the zero order of diffraction) of continuum radiation, and this indicates the formation of HSs in these X-pinch areas. In general, the regions emitting softer radiation (with a maximum of about 50–100 Å) have sizes obviously exceeding the sizes of X-pinch areas radiating in the SXR spectral band ($\lambda < 20$ Å). That is true also for the areas containing HSs. The brightness of HSs in SXR radiation is much higher than the average brightness of radiating area in XUV, but the yield in the SXR range is smaller. Direct comparison of yields in different spectral bands is complicated because of strong nonlinearity of the film response on exposure, and the dependence of the film sensitivity on the wavelength of incidence radiation.

As was mentioned above, some of the experiments were performed using IPs. The main advantage of IPs is a very

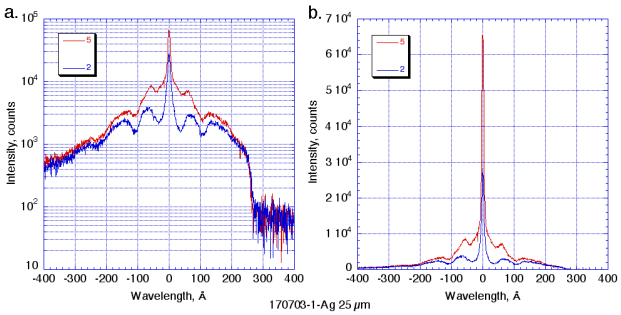

Fig. 9. Lineouts from the TGS spectrum from a 25-μm Ag HXP recorded on (a) Fuji TR IP in logarithmic and (b) linear scales.

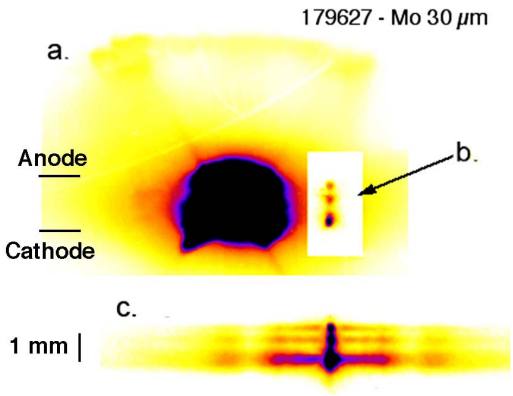

Fig. 10. (a) OP image after the first scan and (b) after the 10th scan of the IP. (c) TGS spectrum recorded on an IP. The spatial scale is the same for all images.

wide dynamic range of the image and a linear response to incident radiation [12]–[15]. Also, the procedure of obtaining and analyzing the image is considerably simplified. The plates can be used many times, they are practically insensitive to visible light and, therefore, do not require protection. The dynamic range of the IPs in our experiments with standard IR readout by a DURR HD-CR35 NDT scanner was about 1000 (Fig. 9) and was limited by noise level. By multiple scanning, the dynamic range was expanded by 1–2 additional orders of magnitude [12]. An example of the images obtained with an OP is shown in Fig. 10(a) and (b). The large illuminated area in Fig. 10(a) was obtained from the first scan; one can see that the image is fully saturated. The same image, but after the tenth scan of the plate, is shown in Fig. 10(b). The fine scale structure of the radiating area is clearly seen on this image; it corresponds to the structure seen for TGS spectrum.

Figs. 11–13 show the HXP spectra from Ag, Al, and Mo HXPs recorded using IPs. They exhibit the same characteristic features of the structure of HXP emitting regions as the images on the UF-4 film, and do not have a characteristic dip due to absorption at the carbon K edge. This is important in our case since, as seen, in particular, in Fig. 12, the Mo X-pinch has emission lines in this part of the spectrum.

However, one should note that the IPs have lower resolution than film (Fig. 14). The main disadvantage of the IPs was the absence of absolute calibration in the spectral range $\lambda > 10$ Å,

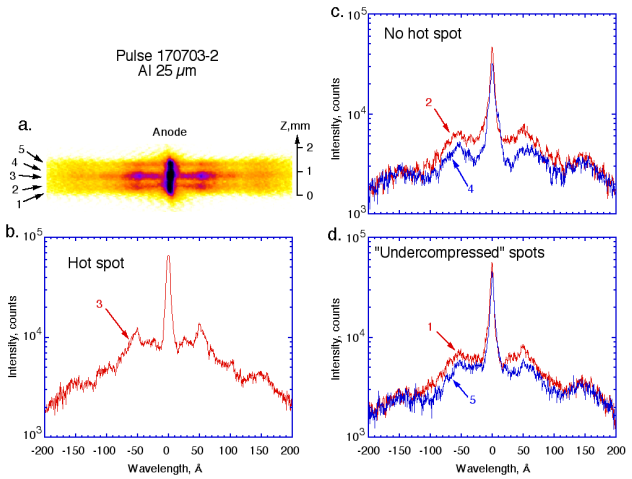

Fig. 11. TGS spectrum from a 25-μm Al HXP recorded on (a) Fuji TR IP and spectrum lineouts [the location number of which corresponds to the position numbers in (a)]. (b) HXP zone with an HS (3). (c) Zones without HSs (2, 4). (d) Zones with "undercompressed" HSs (1, 5).

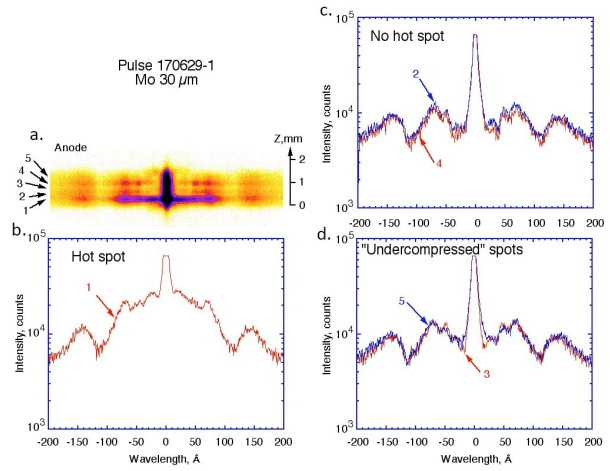

Fig. 12. TGS spectrum from a 30-μm Mo HXP recorded on (a) Fuji TR IP and spectrum lineouts [the location number of which corresponds to the position numbers in (a)]. (b) HXP zone with an HS (1). (c) Zones without HSs (2, 4). (d) Zones with "undercompressed" HSs (3, 5).

TABLE I

EXAMPLES OF RADIATED ENERGY OBTAINED IN HXP WITH DIFFERENT WIRES

material / diameter	Mo 30 μm	W 13 μm	Al 25 μm	Ag 25 μm
energy, J (10 eV < E < 4 keV)	6.2±1.5	4.9±1.5	3.1±1.3	3.0±1.3

which, as mentioned above, makes it impossible to calculate the absolute values of the radiation yield.

To estimate the energy output of HXPs in the wavelength range from 10 to 400 Å, a spectrograph without an input slit was used with the spectra recorded on the calibrated UF-4 film. The total energy yield, calculated taking into account the film

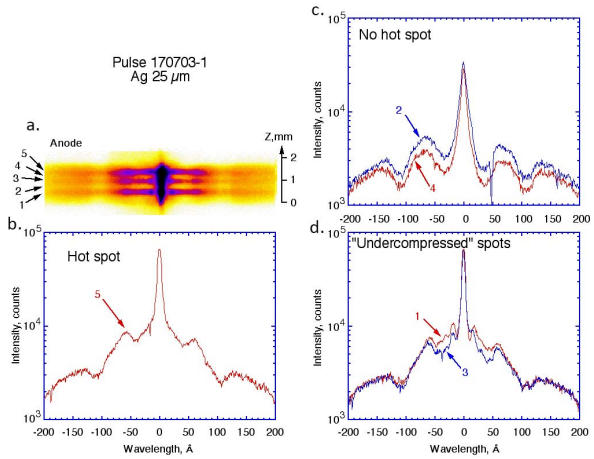

Fig. 13. TGS spectrum from a 25-μm Ag HXP recorded on (a) Fuji TR IP and spectrum lineouts [the location number of which corresponds to the position numbers in (a)]. (b) HXP zone with an HS (5). (c) Zones without HSs (2, 4). (d) Zones with "undercompressed" HSs (1, 3).

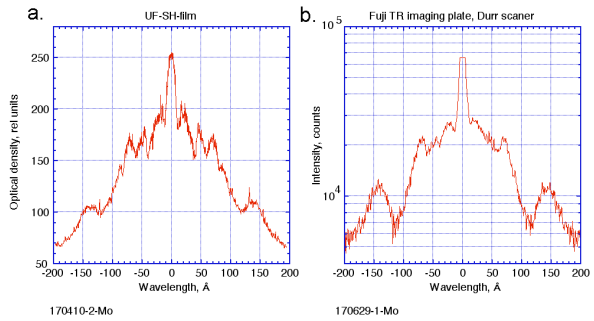

Fig. 14. Comparison of TGS spectra from 30-μm Mo HXPs recorded on (a) UF-4 film and (b) Fuji TR IP.

sensitivity and the experiment geometry, was 3 to 20 J and depended on experimental conditions (these calculations were made for all available data). Detailed results of HXP yield in the XUV spectral band will be published elsewhere. Results of energy measurements in the specific experiments with HXPs shown in Figs. 5–8 using a PCD without a filter are shown in Table I.

IV. CONCLUSION

The first series of experiments using a TGS with spatial resolution showed that the HXP is a bright source of radiation in XUV spectral band (10 Å $< \lambda <$ 400 Å). It was found that total yield of XUV radiation exceeds the SXR ($\lambda <$ 10 Å) yield by 1–2 orders of magnitude. However, "undercompressed" HSs, namely BSs where plasma parameters do not reach HS conditions, also radiate significant amounts of XUV radiation, i.e., comparable yields to HXPs with HSs. It is known that development of the plasma with HS conditions requires fulfillment of the rule $dI/dt > 1$ kA/ns. Even if that criterion is not achieved [16]–[18] the HXP could be used as a source of XUV radiation, but it can be designed to have less stringent requirements for the current driver.

REFERENCES

[1] S. A. Pikuz, T. A. Shelkovenko, and D. A. Hammer, "X-pinch. Part I," *Plasma Phys. Rep.*, vol. 41, no. 4, pp. 291–342, 2015.

[2] S. A. Pikuz, T. A. Shelkovenko, and D. A. Hammer, "X-pinch. Part II," *Plasma Phys. Rep.*, vol. 41, no. 6, pp. 445–491, 2015.

[3] T. A. Shelkovenko, S. A. Pikuz, and D. A. Hammer, "A review of projection radiography of plasma and biological objects in X-pinch radiation," *Plasma Phys. Rep.*, vol. 42, no. 3, pp. 226–268, 2016.

[4] T. A. Shelkovenko, S. A. Pikuz, J. D. Douglas, R. D. McBride, J. B. Greenly, and D. A. Hammer, "Multiwire *X*-pinches at 1-MA current on the COBRA pulsed-power generator," *IEEE Trans. Plasma Sci.*, vol. 34, no. 5, pp. 2336–2341, Oct. 2006.

[5] T. A. Shelkovenko *et al.*, "A source of hard X-ray radiation based on hybrid X pinches," *Phys. Plasmas*, vol. 23, p. 103303, Sep. 2016.

[6] M. Y. Aleksandrov *et al.*, "X-ray spectrometer using a free-standing transmission grating and a microchannel plate as detector for laser plasma studies," *Laser Part. Beams*, vol. 6, no. 3, pp. 561–567, 1988.

[7] K. Eidman *et al.*, "Absolute soft x-ray measurements with a transmission grating spectrometer," *Laser Part. Beams*, vol. 4, nos. 3–4, pp. 521–530, 1986.

[8] *The Diffraction Efficiency of a Transmission Grating*. [Online]. Available: http://henke.lbl.gov/optical_constants/tgrat2.html

[9] A. A. Kologrivov, A. A. Rupasov, and G. V. Sklizkov, "Reconstruction of continuum soft X-ray radiation spectra from registered spectrograms obtained with the use of transmission diffraction grating," Lebedev Phys. Inst., Moscow, Russia, FIAN Rep. 2, 2017.

[10] N. G. Basov, A. Y. Zakharenkov, A. A. Rupasov, and G. V. Sklizkov, *Dense Plasma Diagnostics*, (in Russian). Moscow, Russia: Nauka, 1989.

[11] Y. M. Alexandrov *et al.*, "Investigation of sensitometric characteristics of X-ray photoemulsions in the spectral range of 15–80 Å," *Nucl. Instrum. Methods Phys. Res. A, Accel. Spectrom. Detect. Assoc. Equip.*, vol. 308, pp. 343–346, Oct. 1991.

[12] S. A. Pikuz, T. A. Shelkovenko, D. A. Hammer, and C. L. Hoyt, "Application of a computer radiography based on imaging plates for X-ray diagnostics of X-pinches," in *Proc. 44th Int. Zvenigorod Conf. Plasma Phys. Controlled Fusion*, Feb. 2014, p. 123.

[13] S. G. Gales and C. D. Bentley, "Image plates as x-ray detectors in plasma physics experiments," *Rev. Sci. Instrum.*, vol. 75, no. 10, pp. 4001–4003, 2004.

[14] G. Dunham, E. C. Harding, G. P. Loisel, P. W. Lake, and L. B. Nielsen-Weber, "Cross-calibration of Fuji TR image plate and RAR 2492 x-ray film to determine the response of a DITABIS Super Micron image plate scanner," *Rev. Sci. Instrum.*, vol. 87, no. 11, pp. 11E301-1–11E301-3, 2016.

[15] K. Ren *et al.*, "Calibration of the linear response range of x-ray imaging plates and their reader based on image grayscale values," *Rev. Sci. Instrum.*, vol. 88, no. 8, pp. 083115-1–083115-5, 2017.

[16] R. K. Appartaim and B. T. Maakuu, "X-pinch x-ray sources driven by a 1 μs capacitor discharge," *Phys. Plasmas*, vol. 15, pp. 072703-1–072703-8, Jun. 2008.

[17] A. G. Rousskikh, A. V. Shishlov, A. S. Zhigalin, V. I. Oreshkin, S. A. Chaikovsky, and R. B. Baksht, "Compact X-ray radiograph based on a plasma gun," *Tech. Phys.*, vol. 55, no. 11, pp. 1619–1627, 2010.

[18] F. Zucchini, C. Chauvin, A. Loyen, P. Combes, J. Petit, and S. Bland, "A novel setup for time-resolved X-ray diffraction on gas gun experiments," in *Proc. AIP Conf.*, vol. 1793, 2017, p. 060001.

Authors' photographs and biographies not available at the time of publication.